This article has been accepted for publication in a future issue of this journal, but has not been fully edited. Content may change prior to final publication. Citation information: DOI 10.1109/TIA.2019.2923717, IEEE Transactions on Industry Applications

Design Method of a Direct Drive Permanent Magnet Vernier Generator for a Wind Turbine System

Byungtaek Kim, *Senior Member, IEEE*
Department of Electrical Engineering
Kunsan National University
Gunsan, South Korea
btkim@kunsan.ac.kr

***Abstract*—In this study, a novel design method of a direct-drive (DD) permanent magnet vernier generator (PMVG) is proposed for a gearless, high power and lightweight wind turbine system. Once the maximum power requirement is given, the base and maximum speeds of the generator are firstly obtained from aerodynamic characteristics of wind turbine blade. Then the necessary electrical circuit parameters of the generator are scoped with consideration of the maximum torque per ampere (MTPA) control scheme of a PM generator. To determine the generator geometries satisfying the scoped parameters, the correlations between the parameters and geometries of a PMVG with concentrated windings are deduced. Using the deduced correlations and the obtained parameters, a systematic design procedure of a PMVG is proposed. For a case study, a 5kW DD-PMVG with outer rotor is designed through the proposed method. The performance characteristics of the designed generator are analyzed with finite element (FE) simulations and compared with analytically predicted results. Finally, the experimental results are provided.**

Keywords—direct drive, generator, vernier machine, wind turbine

I. INTRODUCTION

Recently, the interest in renewable energies is very high, and the research and the development on them are more active than ever. Among them, wind-powered generators operate in every size range, from small turbines for battery charging at isolated residences to large wind farms that provide electricity to national electric transmission systems. In particular, wind power generation is being transferred from the ground to the sea, and at the same time, the capacity of generation is growing to the level of gigawatts. These tendencies cause the following compromise; when a mechanical component such as a gear box in an offshore wind turbine breaks down, the maintenance procedure is very complicated and expensive. Therefore, it is beneficial to adopt a direct-drive (DD) generator with no gears, but in this case, the weight of the generator becomes excessively large [1-4]. Hence, to solve these two problems at once, it is necessary to use a DD-generator having much higher power density.

Thus far, various unique machines for the low speed-high torque applications have been presented such as magnetic gears, vernier machines, flux reversal machines and flux switching machines etc. [4-25], and then it is proven that all these machines are classified into the modulation flux machinery which utilizes the magnetic gear effects, alternatively called the flux modulation effects [5]. Especially, it was proven that the permanent magnet (PM) vernier motor, which is a magnetically coupled structure of the magnetic gear and the PM motor, has theoretically much higher output power density because it uses the main PM flux at the same time as the modulation flux [6, 7].

Therefore, several research studies on these kinds of machines have been carried out for generating systems [1, 2], [8-13]. In particular, a magnetic geared machine called a pseudo DD machine was proposed for a wind generator [8] and optimized which has higher torque than the transverse flux machine [1]. In addition, the high possibility of vernier PM machine with dual gap for the DD generator was shown [11, 12], because the structure has the advantage of higher power factor as well as higher power density [14, 15].

On the other hands, the design procedures commonly used for conventional PM machines are not proper for the design of these flux modulation machines. For an example, the most popular design procedure of a conventional PM machine is as follows; The volume of the machine can be initially assumed by using the D^2L-based power equation with the value of torque per rotor volume (TRV), which is actually the air gap volume, obtained from various theoretical predictions and empirical results [16]. Then using the pre-set magnetic and electric loadings, the geometries such as the air gap diameter and the stack length are detailed. From the geometries of the initially designed machine, the circuit parameter values are estimated. The performance characteristics are predicted by solving the equivalent circuit or by using the numerical methods such as FEM. This procedure is repeatedly performed until the desired characteristics are satisfied, commonly coupled with optimization algorithm [26-29]. The effectiveness of this long-established procedure is expected to be quite high for the classical machines, especially for the fixed speed applications. However, the procedure above is not adequate for the flux modulation machines having substantially different TRV values due to unique operating principles. Thus, some studies of design of these machines start with the TRV value chosen from insufficient theoretical prediction [1], [3], [30], which apparently leads to much more repeated adjusting procedures due to the inaccuracy of the TRV value. Furthermore, if the variable speed performances are needed, the design procedure becomes much more complicated and increases uncertainty because the characteristics of both the reactance and the back EMF should be considered simultaneously [31].

In this paper, a novel method for a vernier PM machine design is proposed to avoid the complexity due to repeated design and performance computations and to reduce the uncertainty in the design results. The proposed method is applied to a 5kW DD-PMVG with outer rotor for the laboratory experiments. In the proposed design method, first,

This research was supported by Korea Electric Power Corporation (R18XA04) and by Basic Science Research Program through the National Research Foundation of Korea funded by the Ministry of Education (NRF-2016R1A6A1A03013567).

This article has been accepted for publication in a future issue of this journal, but has not been fully edited. Content may change prior to final publication. Citation information: DOI 10.1109/TIA.2019.2923717, IEEE Transactions on Industry Applications

by considering the machine control schemes of MTPA and the aerodynamic properties of wind power, the equivalent circuit parameter values of the generator meeting torque requirements are scoped. Then, the correlations between the circuit parameters and the geometries of the vernier machine are derived. Using several design constraints such as the maximum surface and volume current densities, the functions expressing the machine volume and the capacity of power converter can be obtained, which suggests the most adequate circuit parameter values. Consequently, the detailed mechanical geometries and electrical specifications of the generator can be determined directly from the suggested circuit parameter values by using the correlations. Finally, the designed outer-rotor, vernier generator is analyzed through finite element (FE) analysis and experimented with a actually produced machine, and the results are compared with analytically predicted ones.

II. Design Consideration for a Direct-Drive Wind Power Generator

A. Calculation of Rotational Speed and Torque

The power transferred to the turbine rotor from wind can be expressed by

$$P_{turbine} = C_p P_{air} = \frac{1}{2} C_p \rho v_w^3 A_{blade} = \frac{1}{2} \pi C_p \rho v_w^3 R_{blade}^2 \tag{1}$$

where P_{air} is the kinetic energy of moving air, C_p is the power coefficient less than 0.59 of Betz limit, A_{blade} is the rotor blade area, R_{blade} is its radius, ρ is the air density approximately 1.225kg/m^3, and v_w is the wind velocity. In the wind turbine system, the cut-in, the rated and the cut-out speeds of wind are specified with consideration of the capacity of wind turbine. In this study, they are set as 3m/s, 9m/s and 15m/s, respectively, demonstrated in Fig. 1(a). The power generation begins at the cut-in speed and increases with a cube of wind speed. After reaching the rated speed, the power is controlled to be constant up to the cut-out speed. In practice, it is convenient to use a tip-speed ratio, λ of (2) to estimate the rotational speed of turbine rotor, where ω_{blade} is the angular speed of the blade rotor.

$$\lambda = \omega_{blade} \frac{R_{blade}}{v_w} \tag{2}$$

The typical characteristics of λ-C_p curve of two-bladed rotor is given by Fig. 1(b), showing the maximum C_p about 0.45 is obtained when the ratio λ is around 7 [32]. Therefore, for a given maximum power 5kW, A_{blade} in (1) is calculated with C_p of 0.45, and thus the radius R_{blade} of blade rotor is also obtained. Finally, the base speed $\omega_{t.base}$ of turbine rotor can be obtained by using (2) and λ of 7, consequently providing the torque of the turbine at each speed, which are given in table I. It should be noted that since the DD-generator is considered, the speed and torque of turbine are same to those of the generator.

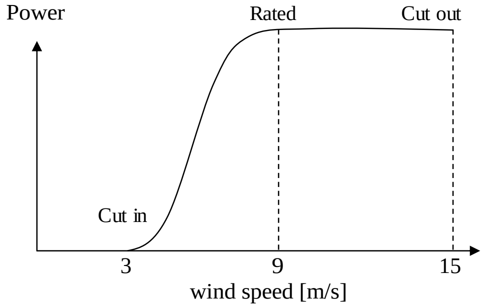

(a) Wind speed vs power characteristics

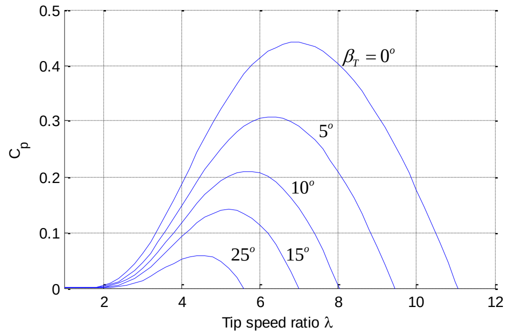

(b) Tip-speed ratio vs C_p characteristics with two bladed-rotor

Fig. 1. Power characteristics of wind power. (β_T: blade pitch angle)

TABLE I. Required Specifications of Wind Power Generator

	Speed (RPM)	Power (kW)	Torque (Nm)
Rated (ω_{base})	213.8	5kW (=P_{max})	236.2
Cut-out (ω_{max})	356.3	5kW	138.6

B. Scoping of Circuit Parameters of PM Generator Considering MTPA Control Scheme

Fig. 2 represents the schematic of a wind turbine system with non-salient PM generator which is represented by the per - phase equivalent circuit consisting of the back electro-motive force(EMF) E_b, the synchronous reactance X_{syn} and the winding resistance R. Neglecting R for convenience, the voltage equation of the generator in DQ-frame can be expressed as (3), and it is depicted as a circle in the DQ-current axes of Fig. 3 whose center, C_v is E_b/X_{syn} of (3). On the other hand, there is the maximum allowable current depending on the thermal capacity of an electrical machine or the power capacity of the converter, and it is represented by a circle with radius I_{max} around the origin. For a non-salient electrical machine, only the q-axis current I_q contribute to torque production, as shown by (4).

$$\left(\frac{V_{ph}}{X_{syn}}\right)^2 = \left(I_d - \frac{E_b}{X_{syn}}\right)^2 + I_q^2 \tag{3}$$

$$I_{\max}^2 = I_d^2 + I_q^2 \tag{4}$$

$$T = \frac{P_m}{\omega_m} = 3 I_q \frac{E_b}{\omega_m} \tag{4}$$

This article has been accepted for publication in a future issue of this journal, but has not been fully edited. Content may change prior to final publication. Citation information: DOI 10.1109/TIA.2019.2923717, IEEE Transactions on Industry Applications

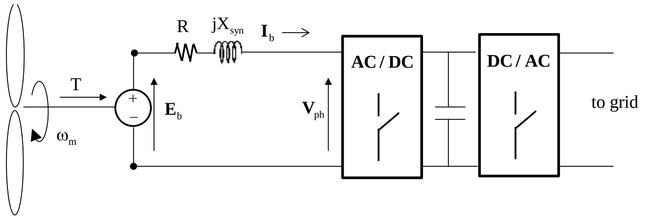

Fig. 2. Wind turbine system with a PM generator

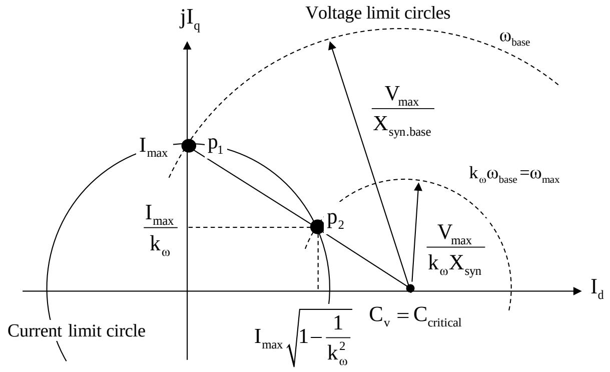

Fig. 3. Operating points for maximum torque production

As is well known, in the maximum torque per ampere (MTPA) control scheme, the radius of the circle V_{ph}/X_{sys} is kept constant as $V_{max}/X_{sys.base}$ to achieve the conditions of I_d=0, that is, $I_q = I_{max}$ until the base speed ω_{base}, so the voltage circle meets with the current circle at p_1 in Fig. 3, and one gets the maximum power $P_{max} = 3I_{max}E_{b.base}$ from (4) at ω_{base}. Above ω_{base}, the radius of voltage limit circle shrinks proportionally as frequency increases, and the voltage circle meets with the current circle at p_2 in Fig.3 at the maximum speed ω_{max}. Because the maximum power P_{max} should be kept from ω_{base} to ω_{max}, it is obvious that I_q at $p_2(\omega_{max})$ should be larger than I_{max}/k_ω in which k_ω is $\omega_{max}/\omega_{base}$. These relations can be expressed by (5).

$$I_q^2(\omega_{max}) = I_{max}^2 - \left(\frac{1}{2C_v}\left(C_v^2 + I_{max}^2 - \left(\frac{V_{max}}{k_\omega X_{syn.base}}\right)^2\right)\right)^2 \geq \left(\frac{I_{max}}{k_\omega}\right)^2 \quad (5)$$

From the right-angled triangle with hypotenuses with p_1, the following (6) is obtained.

$$C_v^2 + I_{max}^2 = \left(\frac{V_{max}}{X_{syn.base}}\right)^2 \quad (6)$$

Using (6), $(V_{max}/k_w X_{syn.base})^2$ in (5) can replaced with $(C_v^2+I_{max}^2)/k_w^2$, and then it can be solved for C_v/I_{max} which is denoted as γ and it is given by (7).

$$\gamma = \frac{C_v}{I_{max}} \leq \sqrt{(k_\omega+1)/(k_\omega-1)} = \gamma_{max} \quad (7)$$

Hence, the available range of γ can be obtained with the both speeds in table I, which gives $\gamma \leq \gamma_{max}$=2.

From the relation (6), $X_{syn.base}$ is given as (8) using γ, and the maximum power P_{max} can be expressed in various form as (9) by using the relations $E_{b.base}=C_v X_{syn.base}$ and $C_v=\gamma I_{max}$. Furthermore, replacing $X_{syn.base}$ in (9) with (8), I_{max} can be obtained as (10).

$$X_{syn.base} = \frac{V_{max}}{I_{max}\sqrt{1+\gamma^2}} \quad (8)$$

$$\begin{aligned} P_{max} &= 3I_{max}E_{b.base} \\ &= 3\gamma I_{max}^2 X_{syn.base} \end{aligned} \quad (9)$$

$$I_{max} = \frac{1}{3}\frac{P_{max}}{V_{max}}\frac{\sqrt{1+\gamma^2}}{\gamma} \quad (10)$$

The maximum phase voltage V_{max} is determined by the DC voltage behind the AC/DC converter in Fig. 2 and is set to $220/\sqrt{3}$ considering the general line voltage. Now, with the voltage V_{max}, the required maximum phase current I_{max} can be obtained using (10) for available γ of (7), and are depicted in Fig. 4. It shows that I_{max} increases as γ decreases, alternatively implying that higher capacity of the power converter is needed as the center of voltage circle is closer to the origin, causing poorer power factor.

In addition, using the obtained I_{max} for the given γ, the parameter C_v is calculated, $X_{syn.base}$ and $E_{b.base}$ are acquired by using (8) and (9) which are given in Fig. 4. It means that there are various available combinations of the maximum current, the back EMF and the synchronous reactance to satisfy the adjustable torque requirements, and it is necessary to find the most suitable combination among them. Furthermore, using (11), the power factor at the base speed under MTPA operation can be estimated and shown in Fig. 4(c). It demonstrates the power factor gets less than 0.5 which is too low when γ is less than 0.6.

$$\cos\theta \approx \frac{E_{b.base}}{\sqrt{E_{b.base}^2 + (X_s I_{max})^2}} \quad (11)$$

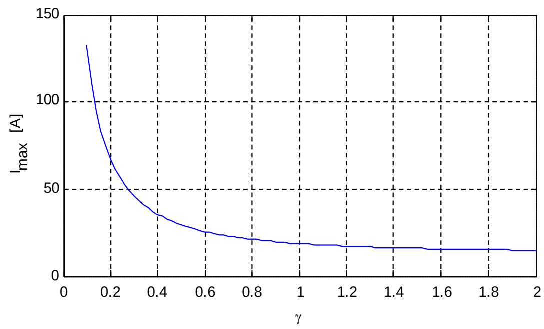

(a) I_{max} vs γ

This article has been accepted for publication in a future issue of this journal, but has not been fully edited. Content may change prior to final publication. Citation information: DOI 10.1109/TIA.2019.2923717, IEEE Transactions on Industry Applications

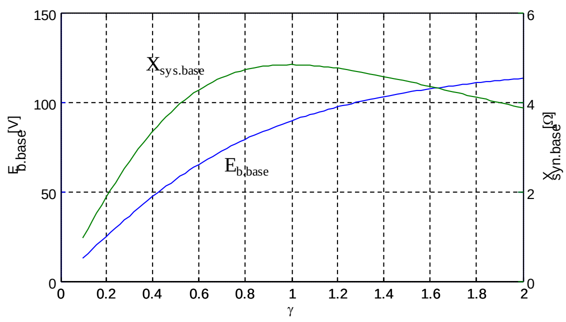

(b) $E_{b.base}$ and $X_{syn.base}$ vs γ

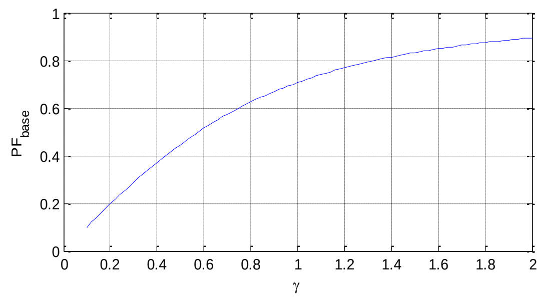

(c) Power factor vs γ

Fig. 4. Necessary maximum current I_{max}, back EMF $E_{b.base}$, synchronous reactance $X_{syn.base}$, and power factor for variation of γ at the base speed

III. Correlations between Circuit Constants and Geometries of a PM Vernier Generator with Concentrated Windings

Once the geometries and electrical specifications of a general PM machine are provided, it is not difficult to calculate the circuit constant values of the machines such as the back EMF and inductances using the classical formula expressed in terms of the geometry of the machine. On the contrary, it is not easy to find the geometries from the circuit constants because the relationship between the two is not a one-to-one correspondence. That is, the number of geometric variables are much more than those of the circuit constants. Moreover, unlike the conventional PM machine, the circuit parameters for the vernier machine has not yet been systematized in the common forms.

In this study, it will be shown the geometric shape of vernier PM generator can be determined from the circuit constants, where several design constraints are used considering current densities and demagnetization of magnet.

To this aim, however, the formula of circuit constants for the PM vernier machine expressed with the geometries are required first. In a PM vernier machine of Fig. 5, the phase coils are wound in Q_s main slots with concentrated winding manner. Since 3 slots in the non-overlapping concentrated winding configurations make up 1 winding pole pair, and thus the winding pole pair p_w is $Q_s/3$. Each main tooth is divided into n_{split} auxiliary teeth, and then the total number of slots Q_{fmp} which is called the flux modulation poles becomes $n_{split}Q_s$. To get vernier effects, the general condition which is p_m-Q_{fmp}=-p_w should be satisfied where p_m is the magnet pole pairs. Solving this condition for p_m, one gets (12) where G_r is commonly called the gear ratio.

$$\begin{aligned} p_m &= Q_{fmp} - p_w = n_{split} Q_s - p_w \\ &= \left(3n_{split} - 1\right) p_w \\ &= G_r p_w \end{aligned} \tag{12}$$

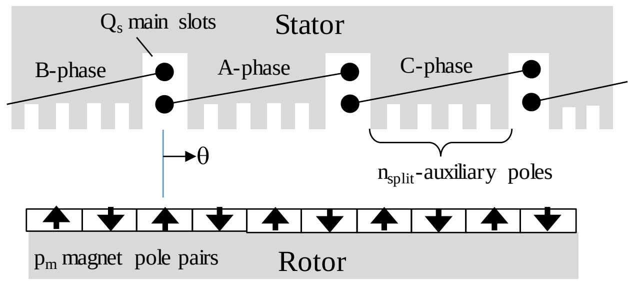

Fig. 5. Schematic of a vernier machine with concentrated windings

A. Back EMF Equation

When the magnetomotive force (MMF) from the p_m magnet pole pairs and the airgap permeance due to Q_{fmp} slots are expressed as

$$F_m \approx F_{1m} \cos p_m \left(\theta - \theta_m\right) \tag{13}$$

$$P_g \approx P_0 - P_1 \cos Q_{fmp} \theta \tag{14}$$

where F_{1m} is $4B_r g_m/\pi\mu_r\mu_0$ and B_r is the residual flux density of PM, μ_0 is permeability of vacuum, μ_r is the recoil permeability of PM, g_m is the magnet thickness. It was revealed for vernier machines, it is desirable to set around 0.5 for c_0 which is the ratio between the slot open width o and the slot pitch [6][15], and in this case, the coefficients P_0 and P_1 of (13) and (14) are given by (15) and (16) respectively in which the coefficient β is given as (17), and g_{m+a} is the effective air gap length, normally the sum of magnet thickness g_m/μ_r and air gap length g_a.

$$\begin{aligned} P_0 &= \frac{\mu_0}{g_{m+a}}\left(1 - 1.6\beta c_0\right) \\ &= \frac{\mu_0}{g_{m+a}}\left(1 - 0.8\beta\right) \quad \left(\text{when } c_0 = 0.5\right) \end{aligned} \tag{15}$$

$$\begin{aligned} P_1 &= \frac{\mu_0}{g_{m+a}} \frac{2\beta}{\pi}\left(\frac{0.39}{0.39 - c_0^{\,2}}\right)\sin\left(1.6\pi c_0\right) \\ &\approx 1.04\frac{\mu_0}{g_{m+a}}\beta \quad \left(\text{when } c_0 = 0.5\right) \end{aligned} \tag{16}$$

$$\begin{aligned} \beta &= \frac{1}{2} - \left\{\sqrt{4 + \left(\frac{o}{g_{m+a}}\right)^2}\right\}^{-1} \\ &= \frac{1}{2} - \left\{\sqrt{4 + \left(\frac{\pi}{2}\frac{D_g}{Q_{fmp} g_{m+a}}\right)^2}\right\}^{-1} \quad \left(\text{when } c_0 = 0.5\right) \end{aligned} \tag{17}$$

Especially, the characteristic of β vs o/g_{m+a} is depicted in Fig. 6. It shows that β increases up to 1/2 as the magnet thickness decreases. However, it is realistic to take around 3~5 for o/g_{m+a} considering the demagnetization of magnet.

This article has been accepted for publication in a future issue of this journal, but has not been fully edited. Content may change prior to final publication. Citation information: DOI 10.1109/TIA.2019.2923717, IEEE Transactions on Industry Applications

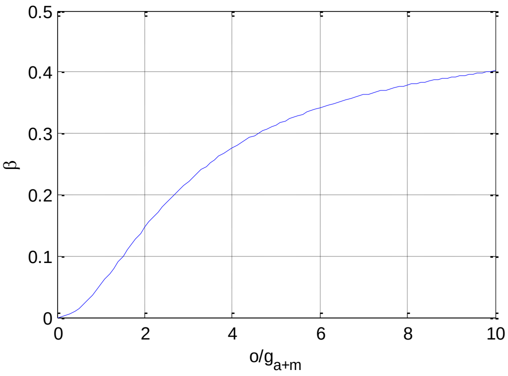

Fig. 6. The characteristic of β vs o/g_{a+m}

Multiplying F_m of (13) and P_g of (14) and neglecting the terms having the small magnitude and speed, the airgap flux density is approximated as (18).

$$B_g \approx F_{1m}P_0 \cos p_m\left(\theta-\theta_m\right)-\frac{F_{1m}P_1}{2}\cos\left(p_w\theta+p_m\theta_m\right) \quad (18)$$

Applying Faraday's law with (18), the back EMF of the concentrated winding with N_{ph} turns per phase can be obtained as

$$\begin{aligned} e_b &= \frac{N_{ph}D_g l_{stk}}{2}\frac{d}{dt}\int_0^{\frac{2\pi}{Q_s}} B_g d\theta \\ &= \sqrt{2}E_b \cos\left(\omega_e t+\varphi\right) \end{aligned} \quad (19)$$

where D_g is the airgap diameter, and l_{stk} is the core stack length and the rms value E_b is given as

$$E_b = \sin\left(\frac{1}{3}\pi\right)\frac{\omega_e}{p_m}\frac{N_{ph}D_g l_{stk}}{\sqrt{2}}F_{1m}\left(P_0+\frac{G_r}{2}P_1\right) \quad (20)$$

From (20), it is seen that P_1 due to the slot harmonic contributes back EMF production, which is called the vernier effects. Using (15) and (16), the back EMF of (20) is rearranged as

$$E_b = \frac{\sqrt{6}}{\pi}\frac{B_r}{\mu_r}\frac{g_m}{g_{m+a}}N_{ph}D_g l_{stk}\left\{1+\left(0.52G_r-0.8\right)\beta\right\}\omega_m \quad (21)$$

which shows well the vernier effects telling that as G_r and β are larger, the back EMF increases.

B. Synchronous Reactance Equation

The synchronous reactance X_{syn} consists of both the air gap and the leakage reactance, and the inductance of the vernier machine is fundamentally same to that of conventional machine. The air gap inductance L_g per phase is dependent on the number of winding turns N_{ph} and the air gap reluctance. The gap inductance of the winding on a tooth can be given as

$$L_{tooth} = \left(\frac{N_{ph}}{Q_s/3}\right)^2\left(\frac{3}{2}\mathcal{R}_{g.slot}\right)^{-1} \quad (22)$$

in which $\mathcal{R}_{tooth}$ is the magnetic reluctance of airgap under one slot pitch area and is given as

$$\mathcal{R}_{tooth} = \frac{g_{m+g}}{\mu_0}\frac{Q_s}{\pi D_g l_{stk}} \quad (23)$$

Now the air gap inductance per phase for a machine with concentrated windings is given by [33]

$$L_{gap} = \frac{Q_s}{3}L_{tooth} = 2\pi\mu_0\left(\frac{N_{ph}}{Q_s}\right)^2\frac{D_g l_{stk}}{g_{m+g}} \quad (24)$$

The major part of leakage inductance of PM machines is the slot leakage and it depends on the slot geometries. For an instance, the slot shape of vernier machine with n_{split}=2 and the leakage flux are illustrated in Fig. 7, and the slot leakage inductance per phase is given as

$$L_{slot} \approx 4\mu_0\left(\frac{N_{ph}}{Q_s}\right)^2 l_{stk}Q_s\left(\frac{d}{o}+\frac{h}{3w}\right) \quad (25)$$

It is realistic to take the ratio of h and w in Fig.7 as 2 for a PM machine with concentrated windings. Since the slot open width o is $0.5\pi D_g/(n_{split}Q_s)$, the width w can be taken as $n_{split}o$ for the room of stator windings, and the height h becomes $\pi D_g/Q_s$. Assuming the height of slot shoe d is same to the slot opening o, the slot leakage inductance per phase of (25) becomes

$$L_{slot} \approx \pi\mu_0\left(\frac{N_{ph}}{Q_s}\right)^2\left(\frac{10}{3}\frac{D_g}{n_{split}o}\right)l_{stk} \quad (26)$$

As mentioned above, o/g_{m+a} is around 3~5, in that case, the slot inductance with n_{split}=2 or 3 is roughly estimated as $L_{slot}\approx 1/3L_{gap}$. Then, the total leakage inductance considering end-turn leakage inductance L_{end} is approximated as

$$L_{leakage} = L_{slot} + L_{end} \approx \frac{1}{2}L_{gap} \quad (27)$$

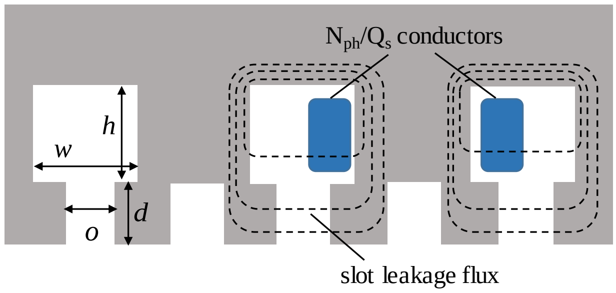

Fig. 7. The sketch of slot leakage with concentrated windings

Consequently, the synchronous reactance is approximated as

$$\begin{aligned} X_{syn} &\approx \frac{3}{2}\omega_e\left(L_{gap}+L_{leakage}\right) \\ &= \frac{9\pi}{2\mu_0}\left(\frac{N_{ph}}{Q_s}\right)^2\frac{D_g l_{stk}}{g_{m+g}}p_m\omega_m \end{aligned} \quad (28)$$

It should be noted that X_{syn} of (28) includes p_m, and p_m is proportional to is G_r from (12), resulting that X_{syn} is directly proportional to G_r. Comparing the reactance X_{syn} with the back EMF E_b of (21), it is apparent that X_{sys} increases much more than E_b as G_r increases, causing worse power factor. Alternatively, due to the relation G_r=n_{split}-1, it is common the power factor gets excessively poor when n_{split} is larger than 3 [6][23].

This article has been accepted for publication in a future issue of this journal, but has not been fully edited. Content may change prior to final publication. Citation information: DOI 10.1109/TIA.2019.2923717, IEEE Transactions on Industry Applications

C. Additional Relations Considering Surface Current Density limitation

The center of the voltage limit C_v which is E_b/X_{syn} is obtained by dividing (21) by (28), and is expressed as

$$C_v = K_{EX}\frac{B_r}{\mu_r}\frac{g_m}{N_{ph}}\frac{p_w}{\left(n_{split}-1/3\right)}\left\{1+\left(0.52G_r-0.8\right)\beta\right\} \quad (29)$$

where the coefficient K_{EX} is $2\sqrt{6}/(3\pi^2\mu_0)$.

Due to the allowable temperature rise of the electrical machines, it is common to set the proper maximum surface current density K_s depending on the cooling capacity. The relation between K_s and the maximum current I_{max} is as follow.

$$I_{max} = \frac{\pi D_g K_s}{6N_{ph}} \quad (30)$$

Therefore, the variable γ which is C_v/I_{max} is also given by

$$\gamma = \left(\frac{6}{\pi}K_{EX}\frac{B_r}{\mu_r}\frac{1}{K_s}\right)\frac{p_w}{\left(n_{split}-1/3\right)}\frac{g_m}{D_g}\left\{1+\left(0.52G_r-0.8\right)\beta\right\} \quad (31)$$

IV. Determination of Geometries of a PMVG

As described in Section II, in order to achieve the performance requirements of the wind turbine, $\gamma \leq \gamma_{max}(=2)$ must be satisfied, and the range of circuit parameters such as $X_{syn.base}$ and $E_{b.base}$ for given γ were specified in Fig. 4. In Section III, the various correlations between the geometric variables and the circuit constants were provided. Especially, it should be noted from (31) that for a given γ, once the magnet material is determined and K_s is specified as a typical value, the variables left to be determined for design are D_g, p_w, g_m, n_{split}, and g_a because G_r and β depend on D_g, n_{split} , and g_a.

Thus, in this study, NdFeB is selected for the PM material whose residual flux density B_r is 1.1T and μ_r is unity. In addition, empirically 30kA/m is chosen as the surface current density K_s [34]. However, for a given γ, the number of circuit constants which are $X_{syn.base}$ and $E_{b.base}$ is still much less than that of the geometric parameters which are D_g, p_w, g_m, n_{split}, and g_a, it is impossible to directly determine the geometries from the electrical parameter value.

In this section, it will be shown that using reasonable mechanical and electrical constraints, the number of shape variables can be reduced, and the most favorable structure is determined among the various possible design candidates.

Since magnet material and surface current density are determined, γ of (31) can be reduced as (32) where K_γ is a constant and G_r is replaced with $3n_{split}$-1.

$$\gamma = K_\gamma\frac{\left\{1+\left(1.56n_{split}-1.32\right)\beta\right\}}{\left(n_{split}-1/3\right)}\frac{p_w g_m}{D_g} \quad (32)$$

It is seen that β of (17) appears in (32). On the other hand, since the magnet thickness g_{m+a} in (17) is slightly greater than g_m, it can be replaced with g_m/0.9, and using $Q_{fmp}=3n_{split}p_w$, β is represented as

$$\beta \approx \frac{1}{2}-\left\{\sqrt{4+\left(\frac{3\pi}{20}\frac{1}{n_{split}}\frac{D_g}{p_w g_m}\right)^2}\right\}^{-1} \quad (33)$$

Now, it should be noted that if the term $D_g/(p_w g_m)$ in (32) and (33) is set as X, the variable γ becomes the function of only n_{split} and X. Therefore, $X(=D_g/(p_w g_m))$ can be calculated by solving (33) for given γ and n_{split}.

On the other hand, replacing the term N_{ph} in the back EMF of (21) with that of (30), the following (34) is obtained where K_E are the constant determined by B_r and K_s.

$$E_b = \frac{K_E}{I_{max}}D_g^2 l_{stk}\left\{1+\left(1.56n_{split}-1.32\right)\beta\right\}\omega_m \quad (34)$$

Also, as shown in Fig. 4, the back-EMF $E_{b.base}$, the required maximum current I_{max}, and the variable β as described above are all a function of γ. Therefore, the equation (34) can be arranged for $D_g^2 l_{skt}$ meaning the air gap volume, as (35) which means the airgap volume can be determined by γ.

$$D_g^2 l_{stk}(\gamma) = \frac{E_{b.base}I_{max}}{K_E\left\{1+\left(1.56n_{split}-1.32\right)\beta\right\}\omega_{m.base}} \quad (35)$$

The above is summarized as follows; $D_g/p_w g_m(=X)$ and β are obtained for available γ using the nonlinear equation (32), and it can be solved with a numerical method such as the simple iterative method [35]. Since $E_{b.base}$ and I_{max} are known for a given γ as shown in Fig. 4, one can calculate $D_g^2 l_{stk}$ using (35), which is very useful information in the design. Fig. 8 represents the calculation results of $p_w g_m/D_g$ and $D_g^2 l_{skt}$ in $\gamma \leq \gamma_{max}$=2 through this method. It shows the necessary volume of the generator with n_{split}=2 is less than that with n_{split}=3 for the region of $0.4 \leq \gamma$. When γ is less than 0.4, the volume with n_{split}=3 can be smaller, but the power factor will be severely poor as described in Fig. 4. Hence, in this study, n_{split} is determined as 2.

From the volume characteristics of n_{split}=2 in Fig. 8(b), it can be also seen that the smaller the value of γ is, the smaller the air gap volume is. This tendency is opposite to the characteristics of γ and the inverter capacity requirement shown in Fig. 4(a), which means that a compromise is required. In other words, the value of γ needs to be strategically determined according to various actual conditions such as the price of the converter and the volume of the generator. In this study, γ was set to 0.6, focusing on the volume of the wind turbine rather than the converter capacity.

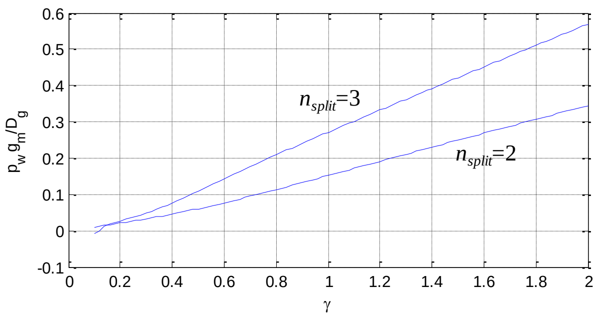

(a) $p_w g_m/D_g$ vs γ

This article has been accepted for publication in a future issue of this journal, but has not been fully edited. Content may change prior to final publication. Citation information: DOI 10.1109/TIA.2019.2923717, IEEE Transactions on Industry Applications

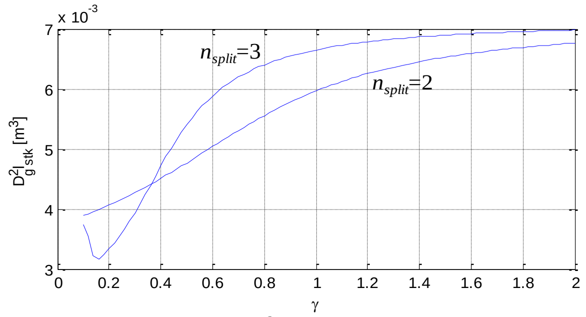

(b) $D^2 l_{stk}$ vs γ

Fig. 8. Geometric variables with γ

The characteristics of $p_w g_m/D_g$ vs γ of Fig. 8(a) is also very useful in the machine design. Since the winding pole pair p_w is an integer, the value of g_m/D_g, that is, the ratio of the magnet thickness to the air gap diameter, can be obtained for p_w from 1 to 3, and the results are depicted in Fig. 9(a). From the results, it can be seen that the larger p_w is, the smaller the thickness of the magnet is, and especially when p_w is 1, the thickness of the magnet becomes excessively thick. Since γ is selected as 0.6, the characteristics of g_m/D_g around the value are redrawn in Fig. 9(b) for convenient investigation. As shown in the figure, when p_w is 3, the thickness of the magnet is the smallest, but when the magnet is excessively thin, there is a high possibility of demagnetization. Therefore, to avoid demagnetization, p_w is chosen as 2, and g_m/D_g becomes 1/30 from Fig. 9(b). At the same time, the value of $D_g^2 l_{stk}$ is $5{\cdot}10^{-3}$m^3 from Fig. 8(b), and the magnet pole pair p_m is 10 from (12).

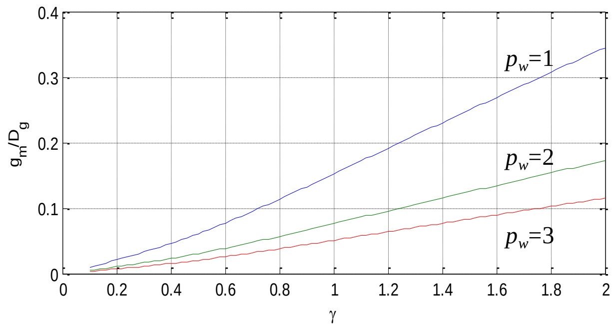

(a) g_m/D_g vs γ with various p_w

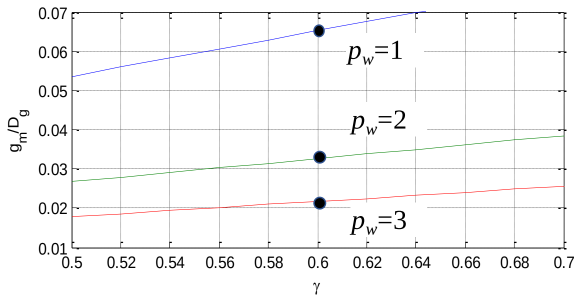

(b) g_m/D_g with various p_w around γ=0.6

Fig. 9. Ratio of g_m and D_g vs γ with various p_w

For the DD machinery with outer rotor, it is beneficial to have a diameter longer than a stack length, and by setting l_{stk}/D_g as 1/2, D_g and l_{stk} can be determined respectively by using the obtained value of $D_g^2 l_{stk}$. Thus, the magnet thickness is obtained from the value of g_m/D_g and the airgap length is also from the selected value 0.9 for g_m/g_{m+a}. Furthermore, using (28), the number of turn per phase N_{ph} is calculated. Now, it can be said that the major geometries of the stator and the rotor are almost determined. In table II, the circuit constants of the generator required to satisfy the specified performances when γ is 0.6, and the shape dimensions determined by the proposed method are summarized.

TABLE II. CALCULATED PARAMETER VALUES WHEN Γ =0.6

Parameter	Value	Parameter	Value
Back EMF $E_{b.base}$	66.3V	Wind. pole pairs p_w	2
Syn. react $X_{sys.base}$	4.27 Ω	Magnet pole pairs p_m	10
Max. current I_{max}	25.2A	Airgap diameter D_g	205mm
n_{split}	2	Stack length l_{stk}	103mm
Phase turns N_{ph}	64	Flux mod. pole Q_{fmp}	12
Main slots Q_s	6	Airgap length g_a	0.8mm
Mag. thickness g_m	6.8mm		

The shapes that have not yet been determined are only the stator slots and the yoke of the stator and rotor, and they can be easily designed using the classical methods. Regarding the shape of the slot, the cross-sectional area of the conductor by is calculated appropriately setting the volume current density of the conductor by the maximum volume current, and then multiplying the number of conductors per slot $2N_{ph}/Q_s$ and the slot occupancy. As mentioned above, since the slot opening ratio c_0 is 0.5, the slot width is calculated from the airgap diameter, and the slot depth is obtained from the calculated slot area. To design the stator and rotor yoke, the magnetic flux density was calculated using the equivalent magnetic circuit of the determined generator, and then the thickness of the yoke of the outer rotor is determined to achieve the magnetic flux density of it as 1.2T. At this time, the influence of the main flux and modulation flux of the vernier motor on the yoke magnetic flux density are considered [24]. Finally, the shape of the determined outer rotor PM vernier generator is shown in Fig. 10.

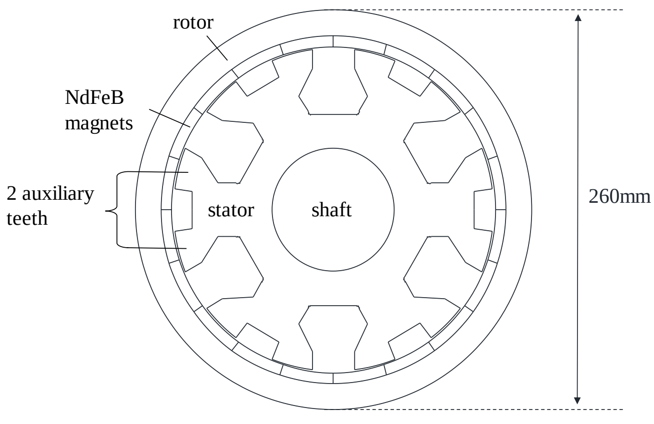

Fig. 10. Designed structure of outer rotor PM vernier generator

V. SIMULATION AND EXPERIMENTAL RESULTS

To prove the validity of the proposed design procedure and the derived equations, the performance characteristics of the designed DD vernier generator of Fig. 10 are analyzed by FEM.

First, the flux distribution and the phase back EMF characteristics without armature currents are calculated at the base speed 214rpm and illustrated in Fig. 11. It shows that the

This article has been accepted for publication in a future issue of this journal, but has not been fully edited. Content may change prior to final publication. Citation information: DOI 10.1109/TIA.2019.2923717, IEEE Transactions on Industry Applications

flux density of teeth is around 1.5T and the density of yokes is lower than 1.2T, meaning that the core parts are properly designed to avoid saturation. Fig. 12 depicts the back-EMF waveforms of three-phase windings, and the rms value estimated from the waveform is 70.5V which is very close to the expected value 66.3V

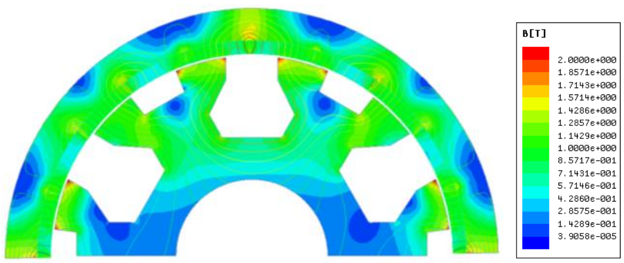

Fig. 11. Flux line and flux density without load currents

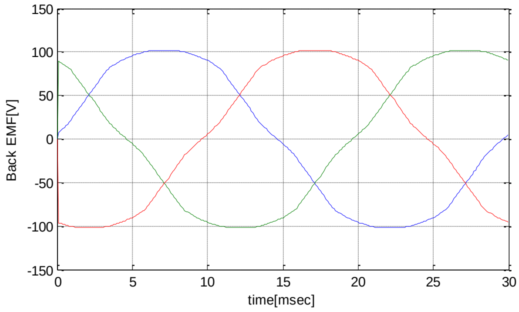

Fig. 12. Back EMF at 214 rpm (FEA results)

Second, to calculate the generator's synchronous reactance X_{syn}, the steady-state currents are calculated at the base speed by the FEM with three-phase windings shorted, which are depicted in Fig. 13. These short currents depends on the back EMF and the synchronous reactance, and to be exact, is given by the relation of $I_{short}=E_b/X_s$. The rms value of the steady state current estimated from the analysis results is about 17.7A. Recalling the back EMF already obtained from FEM is 70.5V, the synchronous reactance is estimated as 4Ω (=70.5V/17.7A) which is also almost the same as the predicted value of 4.2Ω shown in table II. As a result, it can be said that the proposed correlations between the geometries and parameters of the vernier PM machine are very accurate, and the machine design method using the relations are also valid.

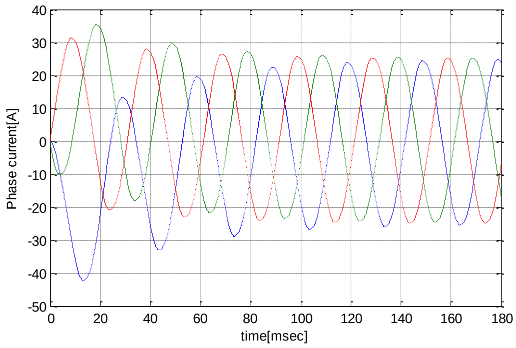

Fig. 13. Phase currents with shorted windings at 214rm (FEA results)

Next, in order to check the output torque characteristics at the base speed, when the maximum phase current I_{max} 25.2A in phase with the back EMF is supplied, the torque and the induced voltage of the winding are analyzed with finite element method. Fig. 14(a) shows the waveform of the torque whose average value is about 249.6Nm close to the design target of 236 Nm for 5 kW. Furthermore, the torque ripple is about 5% which is good enough. Finally, Fig. 14(b) shows the voltage induced in the winding, which refers to the phase voltage to obtain the same current. The effective value of the voltage is 133.2V, which shows good agreement with the design target of $220/\sqrt{3}$ (=127V). It also means that even if the armature current is applied, the estimated values of the reactance and the back EMF are still valid with little saturation effects.

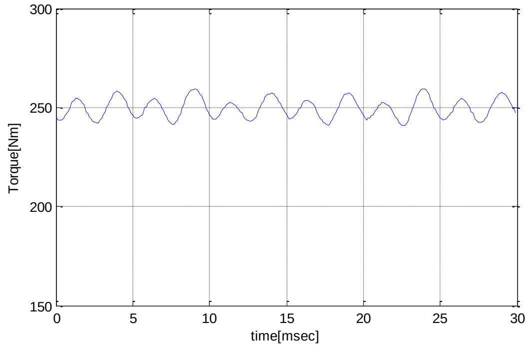

(a) Torque waveforms

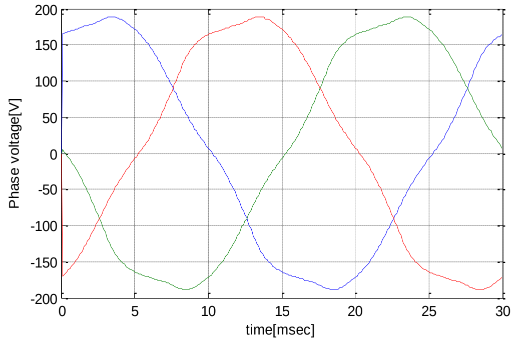

(b) Induced voltage of phase windings

Fig. 14. Load torque and induced voltage characteristics of the designed PM vernier generator (FEA results)

In table III, the simulated values of back EMF, synchronous reactance, the phase voltage and average torque are compared with the predicted values in design procedure, showing very good agreements.

TABLE III. REQUIRED AND OBTAINED CHARATERISTICS OF THE DESIGNED SPM VERNIER GENERATOR AT THE BASE SPEED(213RPM)

Characteristics	Required	FEA	Measured	Err. (%): Exp./Mes.
Torque	236.2Nm	249.6Nm	235.2Nm	5.6
Back EMF	66.3V	70.5V	70.6V	6.3
Syn. reactance	4.2Ω	4.0 Ω	3.91 Ω	4.7
Phase voltage	127V	133.2V	133.0V	4.7

The designed vernier generator with outer-rotor was actually manufactured. Fig. 15 shows the stator and the rotor assembled respectively, and Fig. 16 shows the set-up for experiment. First, the back EMF was measured at the base speed of 214 rpm and the phase voltage waveforms are represented in Fig. 17. The rms value of the back EMF measured is about 71 V, which is very similar to the design value of 66.3 V as well as the finite element analysis results

This article has been accepted for publication in a future issue of this journal, but has not been fully edited. Content may change prior to final publication. Citation information: DOI 10.1109/TIA.2019.2923717, IEEE Transactions on Industry Applications

in Table 1. Next, to estimate the synchronous reactance of the vernier generator, the short-circuit current was measured at the base speed, and the measured current waveforms are shown in Fig. 18. The maximum value 25A of the measured currents is also similar to that of the finite element analysis in Fig. 13. As a result, the estimated synchronous reactance is almost the same as the design value of 4.2 Ω.

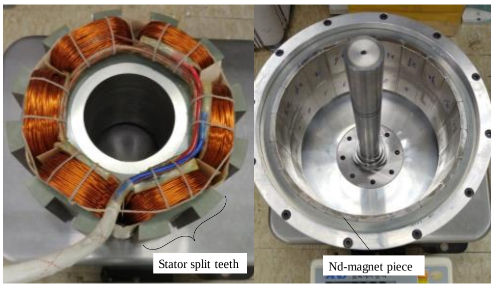

(a) inner stator (b) outer rotor

Fig. 15. Manufactured stator and rotor.

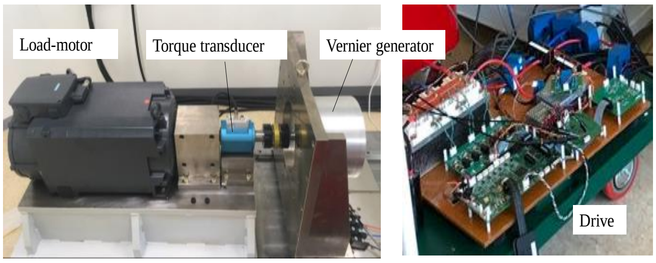

Fig. 16. Set-up for experimental measurement set

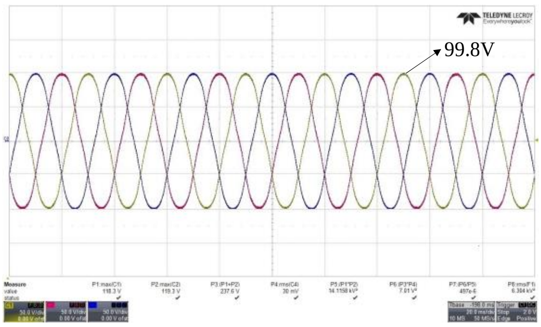

Fig. 17. Phase back EMF at the base speed 214rmp (experimental)

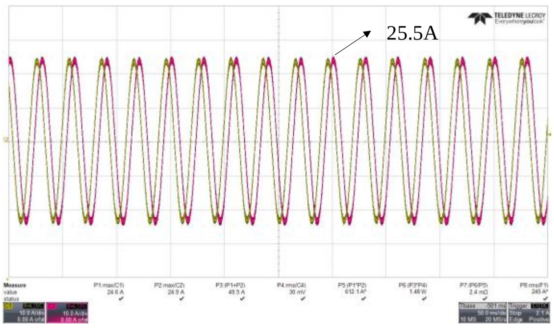

Fig. 18. Phase currents with shorted windings at 214rm (experimental)

Finally, the maximum torque performances for various speeds were tested with the DC link voltage of 340V under MTPA control, as shown in Fig. 19. The torque values at the base speed 213rpm and the maximum speed 356rpm are 235.2Nm and 125.0Nm, respectively. When the measured torque is compared with the design required value, about 10% error occurred at high speed due to mechanical friction and the voltage drop of the cable between the inverter and the generator, but it is considered to be in general good agreement. The efficiency is also excellent, about 90% at the base speed. In addition, it is noteworthy that the torque per air gap volume is very high, 69.2kNm/m^3. Consequently, it is confirmed that the actual PM vernier generator with very high torque density was designed whose characteristics are very close to the predictions through the proposed method.

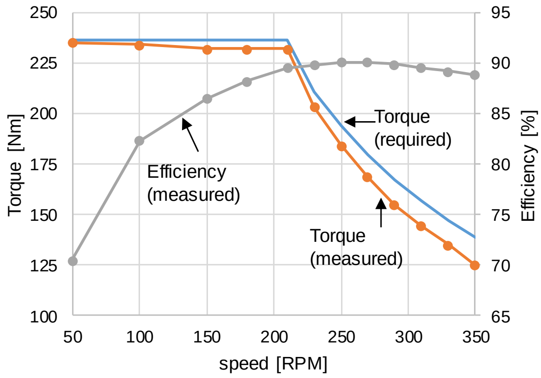

Fig. 19. Torque and efficiency characteristics (experimental)

VI. Conclusion

To improve the problems of the repetitive performance calculation and the resulting inaccuracy in the conventional design procedure of variable-speed electrical machines, this paper proposes a novel design method which is mathematically clear and thus direct and accurate. As a case study, a 5kW direct-drive, outer-rotor PM vernier generator for wind turbine system was designed using the proposed method. The proposed method shows the direct design procedure from choosing the operational speeds of the rotor such as the base and the cut-off speeds to determining the geometries of the generator in details.

The results of this study can be summarized as follows. It has been shown that there are various combinations of circuit constants that satisfy the torque performance required for a wind turbine when a PM generator is represented by a regular electric equivalent circuit. In other words, there may be generators of various different structures. The circuit constant equations expressed in terms of the geometrical structure of the concentrated winding PM vernier generator were derived in consideration of the magnetic gear effects. We have successfully performed a reverse design to determine the shape from the circuit constants by assigning some constraints and reasonable assumptions such as the ratio of the surface current density, the ratio of the gap to the magnet thickness. Then, the reverse design to determine the geometries of a PM vernier generator from the circuit constants has been successfully performed by assigning some constraints and reasonable assumptions such as the ratio of the surface current density, the ratio of the gap to the magnet thickness.

From the design results of the 5 kW DD vernier generators, it was found that 1) the power factor sharply deteriorates as the generator volume decreases, and 2) the generator volume depends on the number of auxiliary teeth of the vernier generators. In this study, it was found that two auxiliary teeth are advantageous for the generator volume. In addition, 3) The number of stator winding poles is closely related to the thickness of the magnets, and therefore the determination of the proper number of winding poles is needed to avoid demagnetization of PM.

By analyzing and testing the performance of the designed DD vernier generator, the following results were obtained. From the FE analysis results, it was confirmed that the back EMF and the synchronous reactance value agree with the predicted value within about 5% error range. It is found that the maximum torque and output of the generator at the base speed are almost similar to 5 kW under the maximum current supply condition. The accuracy of the proposed method was also verified by confirming that the generated voltage at this condition had an error within 5% comparing to the design specification. Finally, we measured the back EMF and the synchronous reactance by testing the vernier generators actually manufactured and confirmed that they are in good agreement with the predicted values at the design stage. In conclusion, it is expected that the proposed systematic design method connecting the circuit constant, required characteristics and geometrical shape of the machine can be very useful for designing various variable speed electrical machines including vernier generators.

REFERENCES

[1] A. Penzkofer and K. Atallah, “Analytical Modeling and Optimization of Pseudo-Direct Drive Permanent Magnet Machines for Large Wind Turbines, IEEE Transactions on Magnetics, Vol. 51, NO. 12, Dec, 2015, p. 8700814

[2] B. Wang, M. Michon, R. Holehouse, K. Atallah , “Dynamic Behaviour of a Multi-MW Wind Turbine”, in *Proc. 2015 IEEE Energy Conversion Congress and Exposition*, pp. 955-962

[3] I. Boldea, A. P. Moldovan and L. Tutelea , “Large wind generators design, performance and control: an overview”, in *Proc. International Symposium on Power Electronics* (Ee), 2017, pp.1-8.

[4] I. Boldea, L. Tutelea, M Topor , “Theoretical characterization of three phase flux reversal machine with rotor-PM flux concentration”, in *Proc. 13th OPTIM*, 2012, pp. 472-476.

[5] Y. Chen, W. Fu, and X Weng, “A Concept of General Flux-Modulated Electric Machines Based on a Unified Theory and Its Application to Developing a Novel Doubly-Fed Dual-Stator Motor”, IEEE Transactions on Industrial Electronics, Vol. 64, No. 12, DEC., 2017, pp. 9914-9923.

[6] Byungtaek Kim and T. A. Lipo, “Operation and design principles of a PM Vernier motors,” IEEE Transactions on Industry Applications, Vol. 50, No. 6, Nov./Dec. 2014, pp. 3656–3663

[7] D. Li, R. Qu, J. Li, L. Xiao, L. Wu, andW. Xu, “Analysis of Torque Capability and Quality in Vernier Permanent-Magnet Machines,” IEEE Transactions on Industry Applications, Vol. 52, No. 1, Jan/Feb 2016, pp. 125-135.

[8] K. Atallah, J. Rens, S. Mezani, and D. Howe, “A Novel “Pseudo” Direct-Drive Brushless Permanent Magnet Machine”, IEEE Transactions on Magnetics, Vol. 44, No. 11, Nov, 2008. pp. 4349-4352

[9] L. Jian, K. T. Chau and J. Z. Jiang, “A Magnetic-Geared Outer-Rotor Permanent-Magnet Brushless Machine for Wind Power Generation”. IEEE Transactions on Industry Applications, Vol. 45, No. 3, 2009, pp. 954-962

[10] J. Li, K. T. Chau, J. Z. Jiang, C. Liu, and W. Li, “A New Efficient Permanent-Magnet Vernier Machine for Wind Power Generation,” IEEE Transactions on Magnetics, Vol. 46, No. 6, June 2010, pp. 1475-1478

[11] S. Jia , R. Qu, J. Li, H. Fang, and D. Li, “A Novel Vernier Reluctance Fully Superconducting Direct Drive Synchronous Generator With Concentrated Windings for Wind Power Application,” IEEE Transactions on Applied Superconductivity, Vol. 26, No. 7, October 2016, p. 5207205

[12] Y. Gao, R. Qu, D. Li, J. Li, and G. Zhou, “Design of a Dual-Stator LTS Vernier Machine for Direct-Drive Wind Power Generation”, IEEE Transactions on Applied Superconductivity, Vol. 26, No. 4, 2016, 5204505

[13] P.R.M. Brooking and M.A. Mueller, “Power Conditioning of the Output from a Linear Vernier Hybrid Permanent Magnet Generator for Use in Direct Drive Wave Energy Converters”, *IEE Proc.-Gener. Transm. Distrib.*, Vol. 152, No. 5, September 2005, pp.673-681.

[14] D. Li, R. Qu, W. Xu, J. Li, and T.A.Lipo, “Design Process of Dual-stator, Spoke-array Vernier PM machines,” in *Proc. IEEE 2014 Energy Conversion Congress and Expo*, 2014, pp. 2350-2357

[15] Byungtaek Kim and T.A Lipo,“Analysis of a PM Vernier Motor with Spoke Structure”, IEEE Transactions on Industry Applications, Vol. 52, 2016, pp. 217-225.

[16] T. J. E. Miller, Brushless Permanent-Magnet and Reluctance Motor Drives, Oxford Science Publications, 1989, pp,. 24

[17] S. L. Ho, S. Niu, and W. N. Fu, “Design and Comparison of Vernier Permanent Magnet Machines”, IEEE Transactions on Magnetics, Vol. 47, No. 10, October 2011, pp. 3280-3283

[18] K. Okada, N. Niguchi, and K. Hirata, “Analysis of a Vernier Motor with Concentrated Windings”, IEEE Transactions on Magnetics, Vol. 49, No. 5, May 2013, pp. 2241-2244

[19] L. Jian, G. Xu, C. Mi, “Analytical Method for Magnetic Field Calculation in a Low-Speed Permanent-Magnet Harmonic Machine”, IEEE Transactions on Energy Conversion, Vol. 26, No. 3, September 2011, pp. 862-870

[20] S. Niu, S. L. Ho, and W. N. Fu, “A Novel Direct-Drive Dual-Structure Permanent Magnet Machine”, IEEE Transactions on Magnetics, Vol. 46, No. 6, June 2010, pp. 2036-2039

[21] X. Li, K. Chau, M. Cheng, B. Kim, and R. D. Lorenz,“Performance Analysis of a Flux-Concentrating Field-Modulated PM Machine for Direct-Drive Applications”, IEEE Transactions on Magnetics, Vol. 51, No. 5, 2015, 8104911

[22] T. Zou , D. Li , R. Qu, D. Jiang , and J. Li , “Advanced High Torque Density PM Vernier Machine With Multiple Working Harmonics,” IEEE Transactions on Industry Applications, Vol. 53, No. 6, Nov/Dec 2017, pp. 5295-5304

[23] Byungteak Kim, “Investigation on Slot–Pole Combinations of a PM Vernier Motor with Fractional-Slot Concentrated Winding Configurations,” Energies, 2017, 10, 1310

[24] Byungtaek Kim, “Design of a PM Vernier Machine with Consideration for Modulation Flux and Comparison with Conventional PM motors,” Energies 2017, 10, 1819

[25] Byungtaek Kim, “Design of a Direct Drive Permanent Magnet Vernier Generator for a Wind Turbine System,” in *Proc. IEEE Energy Convers. Congr. Expo*., 2018, pp. 4275–4282.

[26] K. Yamano, S. Morimoto, M. Sanada, and Y. Inoue, “Basic Study on Design of Surface Permanent Magnet Synchronous Motor Using Design Assist System of PMSM”, 2016 19th International Conference on Electrical Machines and Systems (ICEMS), pp. 1-6

[27] Y. Zhang, N. Liu, S. Guo, J. Tong, and Q. Zhou , “Analysis and Design of Ironless Axial Flux Permanent Magnet Synchronous Motor”, 10th *International Conference on Intelligent Human-Machine Systems and Cybernetics* (IHMSC), 2018, pp. 170-173.

[28] C. Jiang, M. Qiao, P. Zhu, and Q. Zheng, “Design and Verification of High Speed Permanent Magnet Synchronous Motor for Electric Car”, IMCEC 2018, pp. 2371-2375.

[29] F. Parasiliti, M. Villani, S. Lucidi, and F. Rinaldi, “Finite-Element-Based Multiobjective Design Optimization Procedure of Interior Permanent Magnet Synchronous Motors for Wide Constant-Power Region Operation,” IEEE Transactions on Industrial Electronics, Vol. 59, No. 6, June 2012, pp. 2503-2514.

[30] D. Li, R. Qu, W. Xu, J. Li, and T. A. Lipo, “Design process of dual-stator, spoke-array vernier permanent magnet machines”, ECCE 2014, pp. 2350-2357.

[31] B. Kim, “Characteristic analysis of a vernier PM motor considering adjustable speed control”, in *Proc. IEEE ITEC*, 2016, pp. 671-676.

[32] J.G. Slootweg, S. de Hann, H. Polinder, and W. Kling, “General Model for Representing Variable Speed Wind Turbines in Power System Dynamincs Simulations,” IEEE Transactions on Power System, Vol. 18, No. 1, 2003, pp. 144-151

[33] T. A. Lipo, Introduction to AC Machine Design, Wisconsin Power Electronics Research Center, 2007, pp. 155-202

[34] J. Pyrhonen, T. Jokinen, V Hrabovcova, Design of Rotrating Electrical Machines, Weley, 2008, pp. 294

[35] A. Croft and R Davison, M. Hargreaves and J. Flint, Engineering Mathmatics 4/e, Pearson, 2013, pp. 235-236